

Research on Growth Behavior of Calcium Carbonate Scale by Electrochemical Quartz Crystal Microbalance

Junlei Tang¹, Dong Cao¹, Yingying Wang¹, Chamas Mohamad¹, Longju Chen², Hu Wang^{2, *}

¹ School of Chemistry and Chemical Engineering, Southwest Petroleum University, Chengdu 610500, China

² School of Material Science and Engineering, Southwest Petroleum University, Chengdu 610500, China

*E-mail: senty78@126.com

Received: 1 August 2017 / Accepted: 13 October 2017 / Published: 12 November 2017

An electrochemical quartz crystal microbalance (EQCM) was used to evaluate the scaling behavior of CaCO₃ using an electrochemical method in which cathodic potential was applied to the working electrode. Accelerated scaling experiments were performed by varying the temperature and applied potential in a 3.5% NaCl solution containing 200 mg/L Ca²⁺ and 610 mg/L HCO₃⁻. Scale inhibition efficiencies were also compared in the absence and presence of four scale inhibitors, including amino trimethylene phosphonic acid (ATMP), sodium hexametaphosphate (SHMP), 1-hydroxyethylidene-1, 1-diphosphonic acid (HEDP) and copolymer of phosphono and carboxylic acid (POCA). For further investigation of the scale inhibitors' inhibition properties, the growth kinetics of CaCO₃ scale were investigated by injecting scale inhibitors during the scaling formation process. Additionally, to understand the mechanism of scaling inhibition, X-ray diffraction (XRD) and scanning electron microscopy (SEM) were undertaken to analyze and compare the morphologies, particle sizes, and crystal growth of CaCO₃ scale at different conditions.

Keywords: scale inhibitor; calcium carbonate; morphology; crystal growth

1. INTRODUCTION

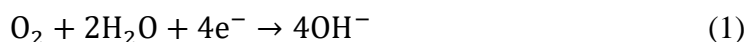
Scaling and corrosion are regarded as two of the most harmful events in many industrial applications [1]. The formation of adhesive mineral deposits on a material surface in liquids is commonly called scaling. The most common forms of scale include CaCO₃, MgCO₃, BaSO₄ and CaSO₄. Undesirable scale deposits often cause various technical problems, such as partial or total obstruction of pipes, which leads to a reduction in flow rate, decrease of heat transfer, failure of valves and clogged filters. Scaling not only causes economic loss but also threatens the production safety.

Calcium carbonate, which is the most familiar scale deposited from natural water, has three major crystalline forms, that is, calcite (rhombohedral), aragonite (orthorhombic) and vaterite (hexagonal). The scaling of calcium carbonate is often influenced by several factors, such as the constituents of the water, the usage of chemicals and the polymorphic composition of the CaCO_3 . Temperature is also a significant parameter, as it increases the rates of nucleation and crystal growth [2,3].

To alleviate the problem of scaling, various methods have been developed. The most common and effective scale control measure is the addition of a scale inhibitor. In application, the goal of utilizing a scale inhibitor is to achieve high efficiency and low cost. In many cases, the concentration of scale inhibitor is strictly limited to within 10 mg/L [4]. The basic functions of a scale inhibitor mainly include the following: (1) In the process of crystallization, negatively charged groups located on the scale inhibitor molecule attack the positive charges on scale nuclei and change the ionic balance, leading to a distortion of crystal growth. (2) Scale inhibitor molecules adsorb onto the crystal forming components and exclude other ions, holding them in solution, preventing particles from fixing to the anionic charges. (3) The precipitation of salts is inhibited at a certain minimum concentration of scale inhibitor known as threshold inhibition, in which case the salt has exceeded its solubility product. (4) Scale inhibitors tend to act as chelating agents when scale inhibitors and scale forming ions are at an equimolar amounts. Commonly used scale inhibitors generally include condensed polyphosphates, organophosphonates, and polyelectrolytes. In practical applications, the most popular scale inhibitors are phosphate-based formulations, which are exactly the scale inhibitors studied in this paper [5].

The methods of evaluating scale inhibitors can be roughly divided into two categories: chemical and non-chemical approaches [6]. Among the non-chemical methods, the electrochemical quartz crystal microbalance (EQCM) has been utilized for many years to promote accelerated scaling by applying an electrochemical potential on a target surface. This technique provides in situ, fast (approximately an hour) and sensitive measurements of the scaling behavior [7].

Ca^{2+} and HCO_3^- ions co-exist in solution to generate CaCO_3 scale in the electrochemically accelerated scaling test [8,9]. The electrochemical process that produces hydroxide ions at the interface of the electrode is represented as follows [10]:



Many studies have been conducted to evaluate scale inhibitors, among which inhibition efficiency, morphology, particle size, crystal growth, and kinetic processes are the most significant parts. These studies have always been conducted at the conditions of natural scaling, a real but time-consuming procedure, which shows obvious disadvantages of experimental time and reproducibility compared to the EQCM method. Especially in the aspects of kinetic studies, EQCM shows a strong advantage. For example, Dimitri [19] observed that the polymers were efficient in delaying or preventing the nucleation/growth process using EQCM. Moreover, C. Garcia [28] used EQCM to evaluate the scale inhibition properties of HEDP and found that this inhibitor has a significant effect on crystal growth. However, only a small number of studies have evaluated the scaling processes in situ using EQCM, which might provide considerably more kinetic information than the other methods.

In this investigation, EQCM was applied to study the scaling behavior of CaCO_3 in a 3.5% NaCl solution. Influential factors, such as temperature, and applied potential were studied. Inhibition

efficiencies were also compared in the absence and presence of four scale inhibitors. For further investigation of their inhibition properties, the growth kinetics of CaCO_3 scale were investigated. Additionally, to understand the mechanisms of scaling inhibition, X-ray diffraction (XRD) and scanning electron microscopy (SEM) were performed to analyze and compare the morphologies, particle sizes, and crystal growth of CaCO_3 scale.

2. EXPERIMENTAL

2.1. Preparation of solutions and scale inhibitors

All of the solutions were prepared with deionized water. The concentration of Ca^{2+} and HCO_3^- ions in all solutions were initially 200 mg/L and 610 mg/L, respectively. The test solution was prepared by dissolving CaCl_2 and NaHCO_3 into a 3.5% NaCl solution. Four commercial scale inhibitors, amino trimethylene phosphonic acid (ATMP), sodium hexametaphosphate (SHMP), 1-hydroxyethylidene-1, 1-diphosphonic acid (HEDP), and copolymer of phosphono and carboxylic acid (POCA) were used to study the scale inhibition behavior. All of the reagents used in the experiments were purchased from Kelong Reagents Co., Ltd. (Sichuan, China).

2.2. Inhibition measurements

The influences of applied potential and temperature were studied by the scaling test. All tests lasted more than 1800 s. Four levels of applied potentials (-0.6, -1.0, -1.4, -1.8 V_{SCE}) and three different temperatures (20, 50, 70 $^\circ\text{C}$) were designed in the electrochemically accelerated test [11,12,13]. A schematic diagram of the test system is shown in Figure 1.

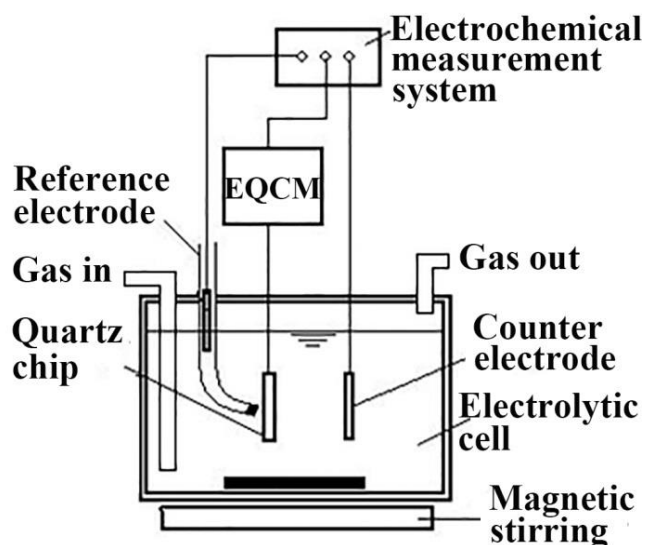


Figure 1. Schematic diagram of the electrochemically accelerated scaling system.

2.3. Evaluation of scale inhibition performance

The methods were designed to evaluate the capabilities of scale inhibitors to prevent the formation of CaCO_3 by measuring the scale mass over time at different concentrations of scale inhibitors [14,15,16]. The concentrations of scale inhibitors were 0, 1, 2, 5, 10 and 20 mg/L, respectively.

2.4. Evaluation of scale deposition kinetics

To understand the reaction kinetics [13], the scaling behavior before and after the additions of the scale inhibitors were recorded. The whole scaling time was divided into two parts: scaling without an inhibitor and scaling with an inhibitor. In other words, during the initial 900 s, the formation of CaCO_3 is totally free of inhibitor; next, a scale inhibitor at a concentration of 10 mg/L is added at the scaling time of 900 s.

2.5. SEM and XRD analysis of the scale crystals

The morphological changes of the calcium carbonate crystals in the presence of different scale inhibitors were examined using a JEOL JSM-6510LV scanning electron microscope (SEM). The CaCO_3 crystals were also characterized using a PANalytical X'Pert PRO MPD X-ray diffraction (XRD) instrument [17]. The powder (XRD) patterns were collected in the 2θ angular range of 10° to 80° with a 2θ scan step of 0.015° and step time of 0.2 s using a $\text{CuK}\alpha 1$ radiation source ($\lambda = 0.154056$ nm) and a Ni filter. The computer program JADE with a PDF card was used to identify the CaCO_3 pattern.

3. RESULTS AND DISCUSSION

3.1. Influence of parameters on scaling

In EQCM measurements, the scaling temperature, applied potential and scaling time have remarkable effects on the scale. Figure 2 shows the influence of temperature on scaling, as determined using EQCM. At each temperature, the scaling amount gradually increases with time. The Scale mass-Time curve is nearly linear. It is also shown that as the temperature rises, the slope of scaling curve rapidly increases, indicating that the higher the temperature is, the faster the scaling process is. It is commonly believed that as the temperature increases, the scaling process increases exponentially, which obeys the Arrhenius equation [18].

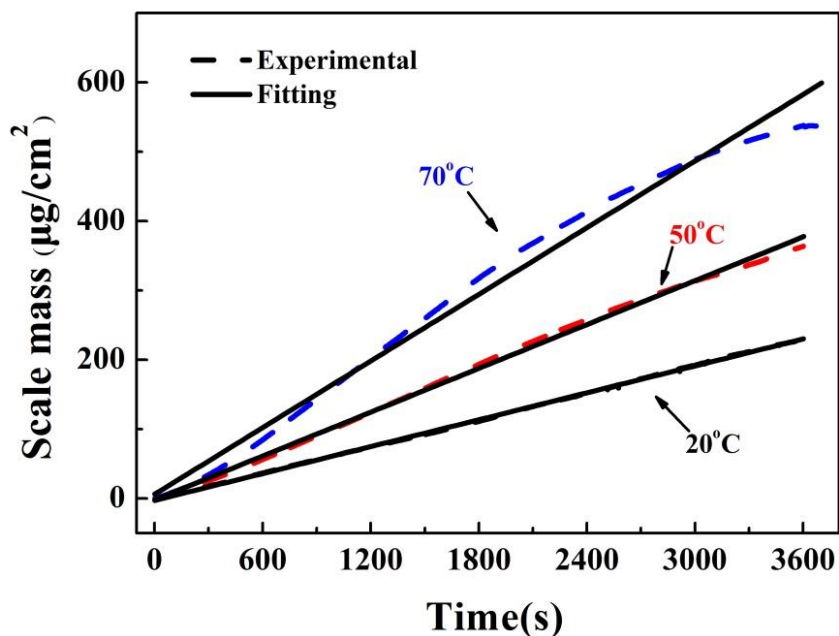


Figure 2. Scale mass-Time curves at different scaling temperatures (20, 50, 70 °C): scaling time (3600 s), applied potential (-1.4 V_{SCE}).

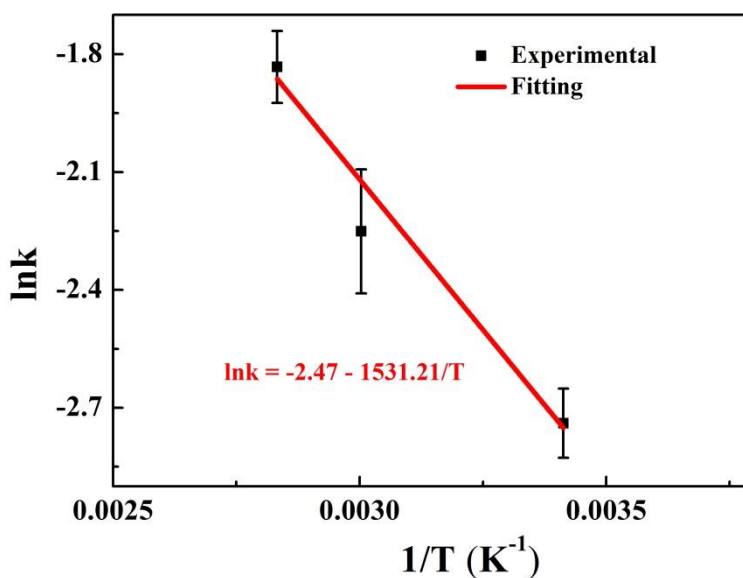


Figure 3. Validation of the growth rate of CaCO₃ versus scaling temperature by using the Arrhenius equation.

The growth rate of CaCO₃ scale obtained from the slope of fitting curves was used to calculate the apparent activation energy by the Arrhenius equation.

$$k = Ae^{-\frac{E_a}{RT}} \tag{3}$$

where k is the reaction rate constant, which depends on the temperature, A denotes the pre-exponential factor, T represents the thermodynamic temperature, °K, R is the molar gas constant, and E_a stands for the apparent activation energy.

By plotting $\ln k$ versus $1/T$, E_a can be calculated as follows.

$$\ln k = \ln k_0 - \frac{E_a}{RT} \tag{4}$$

$$E_a = -12.73 \text{ kJ/mol} \tag{5}$$

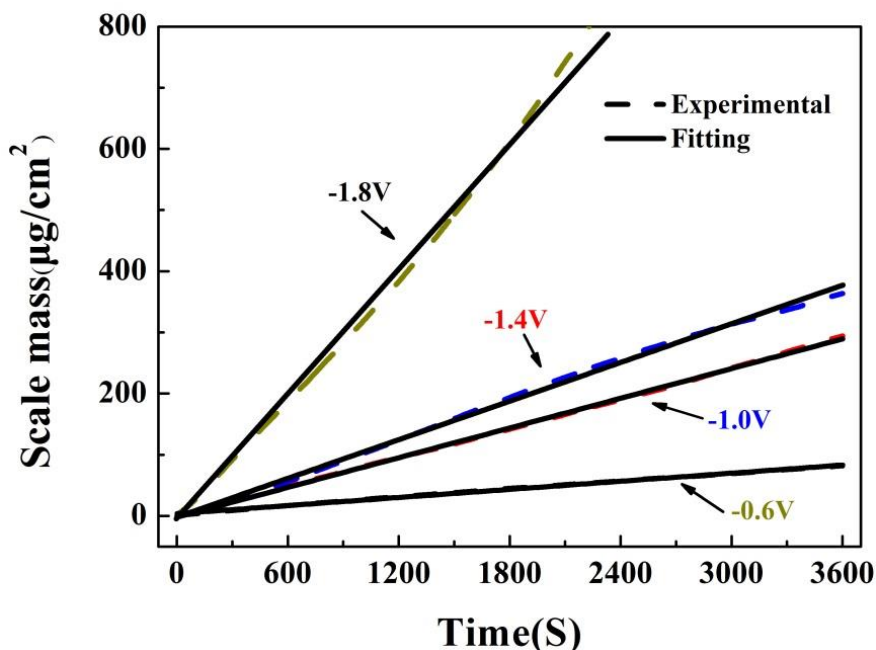


Figure 4. Scale mass-Time curves at different applied potentials (-0.6, -1.0, -1.4, 1.8 V_{SCE}): scaling temperature ($50\text{ }^\circ\text{C}$), and scaling time (3600 s).

The applied potential also has a pronounced influence on scaling. The effect of applied potential on scaling is shown in Figure 3. The maximum growth rate can be observed at $-1.8\text{ }V_{SCE}$. Within the investigated applied potential range of $-0.6\text{ }V_{SCE}$ to $-1.8\text{ }V_{SCE}$, the higher the potential was applied, the slower the growth rate became. The reason for this behavior can be that a higher applied potential provides a larger driving force to the ions to overcome the activation energy of the scaling reaction [19].

The deposition equation of electroplating was adopted to analyze the relationship between the deposition rate of CaCO_3 and the cathode current density [20].

$$V = \frac{100KD_k\eta_k}{\rho} \tag{6}$$

where V is the deposition rate of CaCO_3 (mm/h), K is electrochemical equivalent (g/A h), D_k is the cathode current density (A/dm^2), η_k is the current efficiency (%) and ρ is the density of CaCO_3 (g/cm^3).

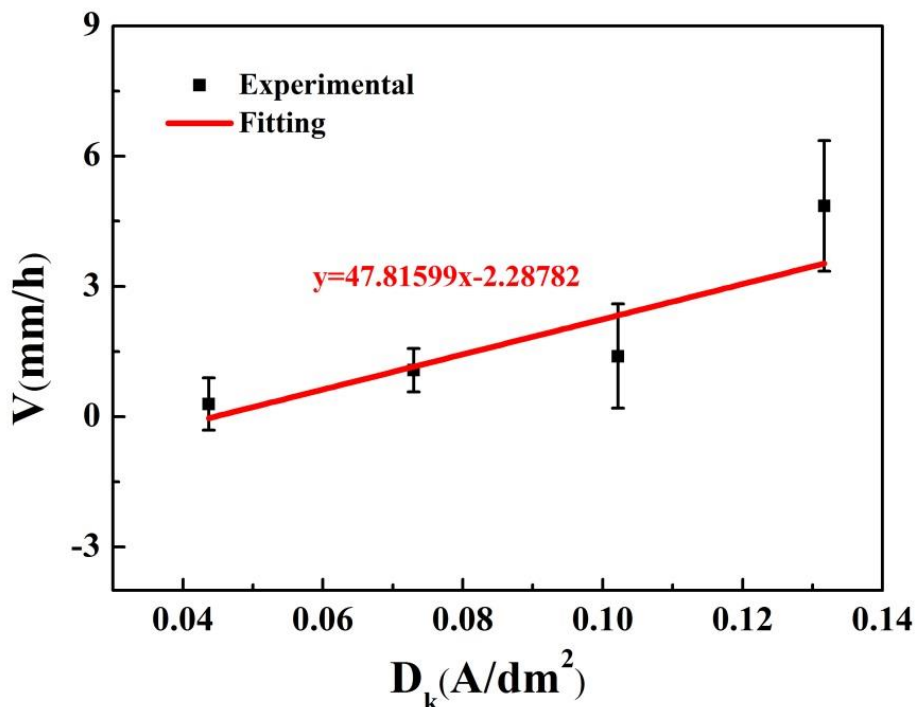


Figure 5. Fitting curves of the deposition rate versus the current density.

$$V = 47.81599D_k - 2.28782 \tag{7}$$

Equation (7) presents the relationship between V and D_k using a linear fitting. To a certain degree, the intercept can be ignored, and the orthogonal equation can thus be obtained:

$$\frac{V}{D_k} = 47.81599 \tag{8}$$

The cathode current efficiency is calculated by using the deposition rate equation:

$$\eta_k = 69.71\% \tag{9}$$

In electroplating, the cathode current efficiency is considered as a significant index for the current utilization percentage, the ratio of the real mass and the theoretical mass of electroplate product. The difference is primarily due to side reactions. Comparatively, for the deposition of CaCO_3 scale, the cathode current efficiency can be influenced by the interfacial pH [21,22], transportation of scale components and the conductivity of the gold surface.

3.2. Influence of scale inhibitors on scaling

Adding a scale inhibitor is one of the most effective ways of alleviating scaling [19,23]. In this study, the scaling and inhibition processes were recorded in the absence and presence of different concentrations of four scale inhibitors, ATMP, POCA, HEDP and SHMP, by EQCM at 50 °C and a potential of -1.4 V_{SCE} .

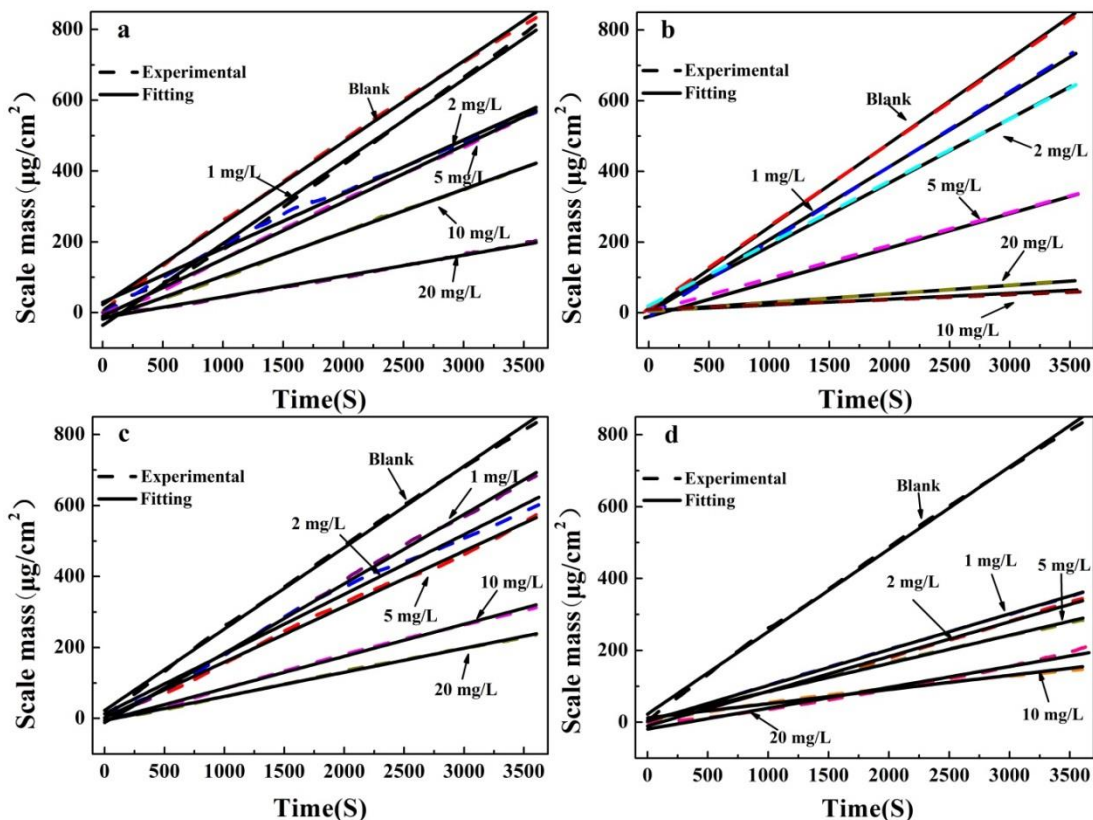


Figure 6. Scale mass-Time curves in the presence of different scale inhibitors, (a) ATMP, (b) HEDP, (c) POCA, (d) SHMP, with concentrations of 0, 1, 2, 5, 10 and 20 mg/L: scaling temperature (50 °C), applied potential (-1.4 V_{SCE}), and scaling time (3600 s).

It can be seen in Figure 6 that the scale mass decreases remarkably with the presence of a scale inhibitor. Additionally, the concentration of scale inhibitor has a notable influence on the scaling process. For example, in Figure 6a, the scale amount continuously rises with the scaling time. The curve of Scale mass-Time obeys a linear relationship. Although it still obeys a linear relationship in the presence of an inhibitor, the inhibitor induces a sharp decline of the slope of the curve, indicating that the scaling rate has been lowered by the inhibition effect of the scale inhibitor. With an increase of the inhibitor concentration, the slope declines and scaling rate is slower, which implies that the inhibition effect is more apparent at higher inhibitor concentrations. The inhibition efficiency of a scale inhibitor can be calculated using the following equation:

$$\eta = \frac{S_{\text{uninh}} - S_{\text{inh}}}{S_{\text{uninh}}} \times 100\% \tag{10}$$

where η is the inhibition efficiency (%), S_{uninh} is the growth rate without the scale inhibitor ($\mu\text{g}/\text{cm}^2 \cdot \text{s}$) and S_{inh} is the growth rate in the presence of the scale inhibitor ($\mu\text{g}/\text{cm}^2 \cdot \text{s}$).

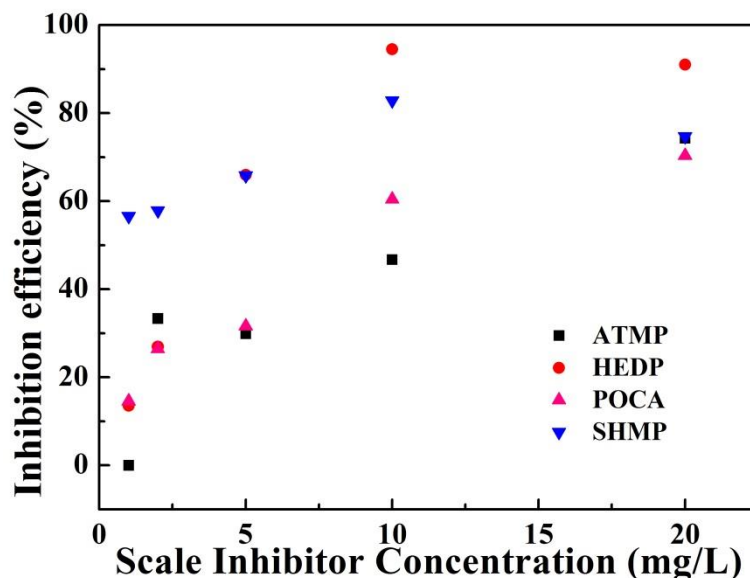


Figure 7. Inhibition efficiencies of scale inhibitors at different concentrations calculated using the fitting growth rate equation: concentrations (0, 1, 2, 5, 10, 20 mg/L), scaling time (3600 s); scaling temperature (50 °C), applied potential (-1.4 V_{SCE}).

The inhibition efficiencies in a static solution with the addition of scale inhibitors are shown in Figure 7. SHMP exhibits a stable inhibition property and reaches a peak value at 10 mg/L. HEDP also reaches the best inhibition efficiency at 10 mg/L. Additionally, the inhibition efficiencies of HEDP and SHMP are better than POCA and ATMP at almost all concentrations.

3.3. Crystallization kinetics of CaCO₃

To understand the mechanism of scale inhibitors, kinetic experiments were performed in a static condition with the addition of scale inhibitors at a concentration of 10 mg/L and an accelerated scaling time of 900 s. As is shown in Figure 8, the slopes of the curves (the scaling rate) in every experiment decrease dramatically with the addition of scale inhibitors, implying the alleviation of the growth of CaCO₃ scale. As it has been reported, from the kinetic aspects, the scaling process of CaCO₃ in the presence of scale inhibitors can be divided into four stages [13,24,25,28]. The first stage is scaling in the absence of a scale inhibitor, featuring the free growth stage of CaCO₃ scale. The second and third stages are unstable diffusion and stable diffusion of the scale inhibitor, respectively. The period between these two stages is defined as the diffusion time, which is also considered to be a critical index to evaluate scale inhibitor. The fourth stage is the stable reaction of scale inhibitor.

As is shown in Figure 8, the curves of every case of the control experiment are characterized by the appearance of two regions. To elucidate the crystallization kinetics and compare the four scale inhibitors, the inhibition efficiencies of scale inhibitors were calculated using the following equation:

$$\eta = \frac{K_{\text{uninh}} - K_{\text{inh}}}{K_{\text{uninh}}} \times 100\% \quad (11)$$

where η is inhibition efficiency of the scale inhibitor (%), K_{uninh} is the slope, obtained by linear fitting, of the curve in the absence of the scale inhibitor ($\mu\text{g}/\text{cm}^2 \text{ s}$) and K_{inh} is slope, obtained by

linear fitting, of the curve after the addition of the scale inhibitor ($\mu\text{g}/\text{cm}^2.\text{s}$). In addition, the linear fitting equation is as follows:

$$y = ax + b \tag{12}$$

where a is the slope mentioned above representing the growth rate of CaCO_3 scale ($\mu\text{g}/\text{cm}^2.\text{s}$), and b is the intercept.

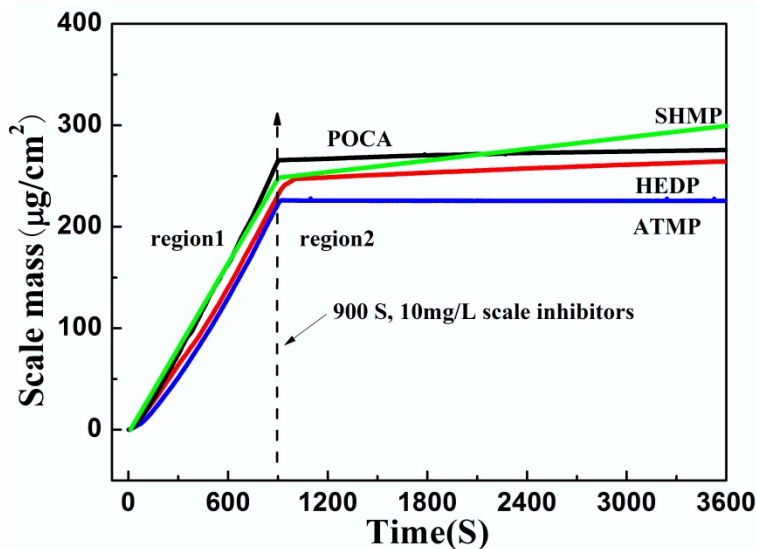


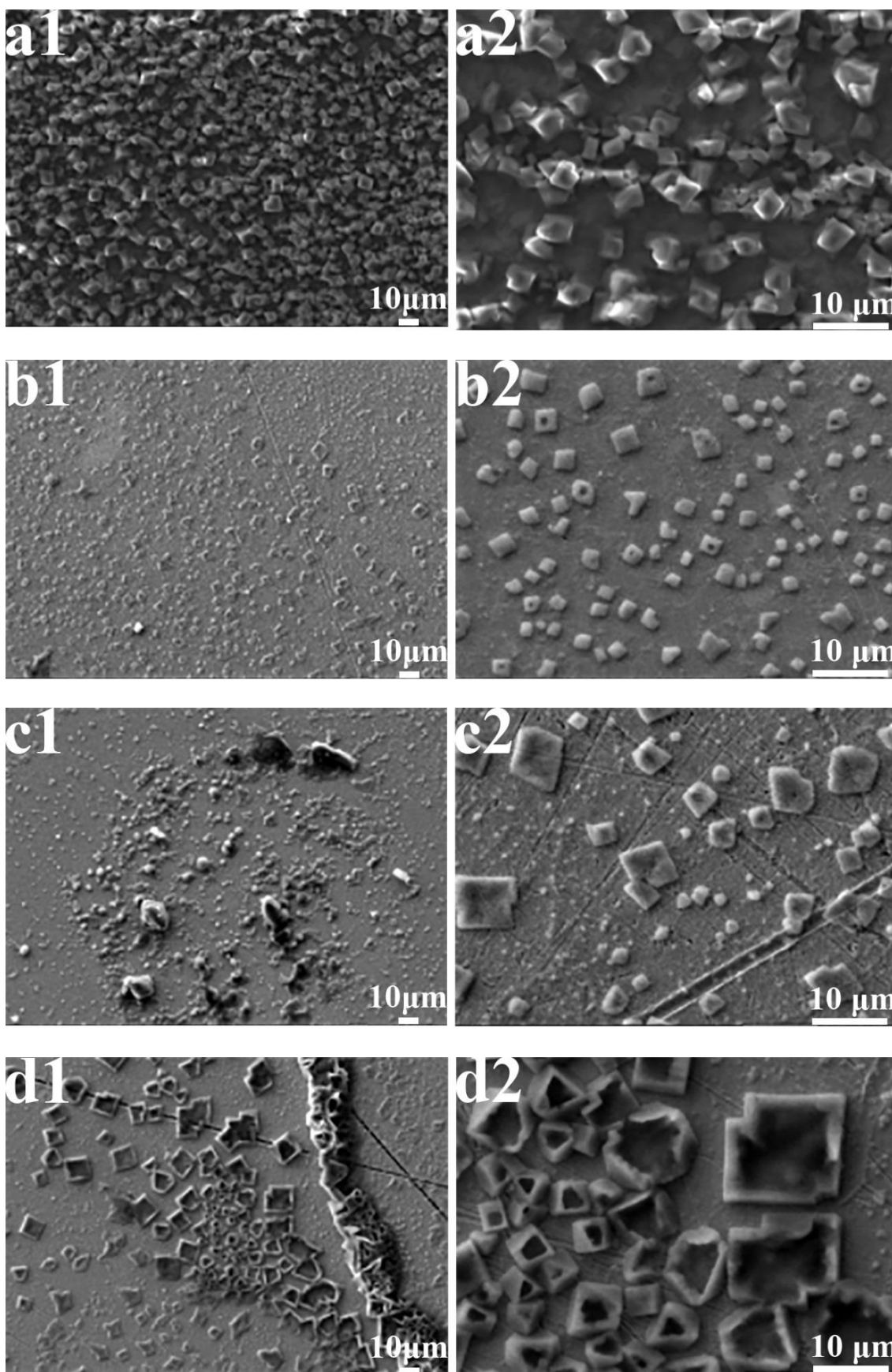
Figure 8. Scale mass-Time curves in the presence of scale inhibitors (10 mg/L) at approximately 900 s: scaling temperature (50 °C), applied potential (-1.4 V_{SCE}), scaling time (3600 s).

Table 1. Fitting results of scaling curves recorded with the addition of scale inhibitors at the accelerated scaling time of 900 s: 10 mg/L scale inhibitors ((a) ATMP, (b) HEDP, (c) POCA, (d) SHMP).

| Scale inhibitors (10 mg/L) | | POCA | HEDP | ATMP | SHMP |
|----------------------------|----------------|---------|---------|---------|---------|
| Region1 | a ₁ | 0.166 | 0.153 | 0.135 | 0.158 |
| | b ₁ | -5.917 | -10.240 | -12.395 | -8.314 |
| Region2 | a ₂ | 0.00248 | 0.00937 | 0.00373 | 0.0178 |
| | b ₂ | 260.955 | 238.202 | 222.654 | 230.997 |
| η (%) | | 98.5 | 93.9 | 97.2 | 88.7 |

As is shown in Table 1, the inhibition efficiencies of the scale inhibitors are calculated two regions before and after adding the scale inhibitors. For region 1, the slopes of Scale mass-Time curves before the addition of four scale inhibitors present some differences owing to certain external factors. Region 2 represents the growth of CaCO_3 under the inhibition of the four scale inhibitors. The values of a₂ in the presence of POCA, HEDP and ATMP are in almost the same order of magnitude, while in the case of SHMP is up to one order of magnitude higher. From the aspect of inhibition efficiency, POCA, HEDP, ATMP and SHMP are almost at the same level, but the order from high to low is POCA, ATMP, HEDP and SHMP.

3.4. Scale micromorphology



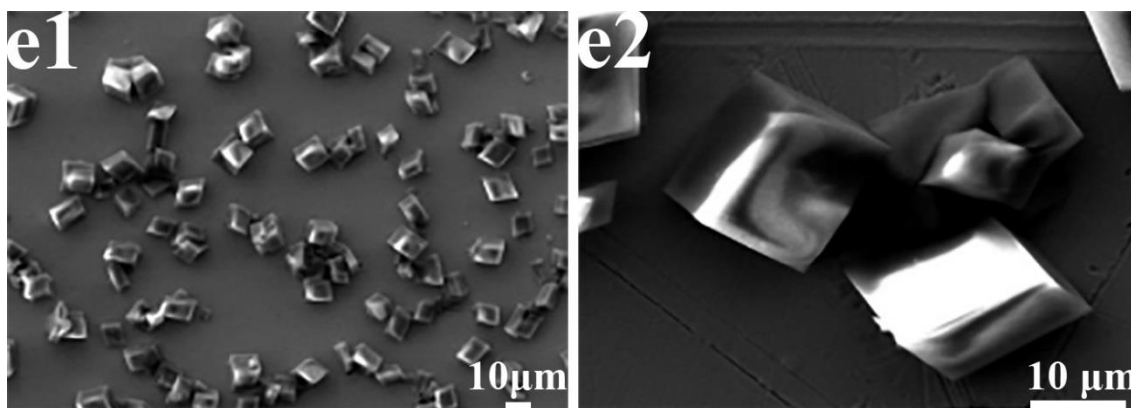


Figure 9. SEM images of CaCO_3 scale obtained from the electrochemically accelerated test in the absence and presence of scale inhibitor (10 mg/L): (a)Blank, (b)ATMP, (c)HEDP, (d)POCA, (e)SHMP, scaling temperature (50 °C), applied potential (-1.4 V_{SCE}), scaling time (3600 s).

Evidence to elaborate the effect of a scale inhibitor on the CaCO_3 crystals is also available in terms of SEM observations [26,27]. As shown in Figure 8, the electrode is almost totally covered by rhombohedral CaCO_3 crystals, which is the classic morphology of calcite (Figure 9a) in the absence of a scale inhibitor. Comparatively, a dramatic change of particle size, amount, morphology and uniformity is observed in the presence of ATMP. The electrode is only partially covered. The amount and particle size of CaCO_3 decreases notably (Figure 9b). It can be seen that in the presence of HEDP (Figure 9c), CaCO_3 exhibits an irregular rhombohedral shape [28], in which the scale on electrode surface distributes unevenly. In the case of POCA (Figure 9d), the particle size of CaCO_3 decreases slightly, and the morphology is modified from the standard rhombohedral form to an irregular rhombohedral form with a void, indicating that POCA has excellent lattice distortion ability. For SHMP (Figure 9e), the scale amount decreases and the electrode is partially exposed. While there is no obvious change of the particle size and morphology of CaCO_3 crystals [27].

The CaCO_3 crystals were also characterized by XRD analysis. To quantify the particle size of CaCO_3 crystals, the diameter was calculated by using the Scherrer equation (12):

$$D = \frac{K\gamma}{B\cos\theta} \quad (12)$$

where K is the Scherrer constant (equal to 0.89), B is the FWHM of the diffraction peak, D is the average thickness of a crystal grain perpendicular to the direction of the crystal face (nm), B full width at half maximum (FWHM, rad), θ is the diffraction angle (rad) and γ is the wavelength of the X-ray (0.154 nm).

As is shown in Table 2, the diameters of CaCO_3 crystals with and without scale inhibitors were 75.5 nm (Blank), 32.6 nm (ATMP), 33.7 nm (HEDP), 68.3 nm (POCA) and 75.5 nm (SHMP). In this calculation, ATMP and HEDP were revealed as the most effective scale inhibitors compared to the obscure changes of POCA and SHMP based on the SEM results.

According to Figure 9 and Table 2, ATMP and HEDP appeared to be excellent for distorting the crystal growth and diminishing the particle sizes of CaCO_3 . The morphology and particle sizes of

CaCO₃ in the case of ATMP resembled those of HDEP but with a minute void and they had comparatively smaller crystal surfaces, signifying a subtle difference of inhibition between these two organic phosphate scale inhibitors. The SEM image of CaCO₃ obtained in the presence of POCA displayed an obvious variation in morphology. Unlike the standard rhombohedral structure of the blank sample, the structure of the CaCO₃ crystals was irregular and contained a significant void, resembling the morphology of the case of ATMP but with an inconspicuous change in particle size. Less obvious variations in both morphology and particle size revealed the deficiency of SHMP in the inhibition of crystal growth.

Table 2. Calculation of the particle size of CaCO₃ crystals by using the Scherrer equation.

| Scale inhibitors | Parameter | | |
|------------------|------------|-------|-------|
| | 2θ(Degree) | FWHM | D(nm) |
| Blank | 26.866 | 0.107 | 75.5 |
| ATMP | 26.866 | 0.248 | 32.6 |
| HEDP | 31.896 | 0.242 | 33.7 |
| POCA | 29.657 | 0.119 | 68.8 |
| SHMP | 26.866 | 0.107 | 75.5 |

3.5. Microstructure analysis

To identify the microstructure of the CaCO₃ crystals in the absence and presence of inhibitors, XRD measurements were performed. The spectra are shown in Figure 10. Calcite is the most thermodynamically stable, while vaterite is the least stable form of the three polymorphic forms of CaCO₃. In this study, the main crystal form is calcite due to the effect of temperature and applied potential [18,26]. In the absence of a scale inhibitor, the main XRD peak is from calcite crystals at 26.866°, which corresponds to the calcite crystal faces (002), indicating that calcite is the main crystal form in the absence of a scale inhibitor. With SHMP, (002) is still the main crystal face, and the diffraction peak exerts a high strength at the same diffraction angle, meaning that SHMP makes no changes to the crystal growth of CaCO₃. Two weak diffraction peaks are observed at 26.866° and 31.896° corresponding to the calcite crystal faces (002) and (212), respectively, which signifies the high efficiency of ATMP with respect to lattice distortion. In the presence of HEDP, only the (212) plane can be observed. In addition, the peak is weaker compared to that of the blank sample, which agrees with its SEM image. In the case of POCA, two diffraction peaks are observed corresponding to the crystal faces (220) and (212) at 29.657° and 31.896°, respectively.

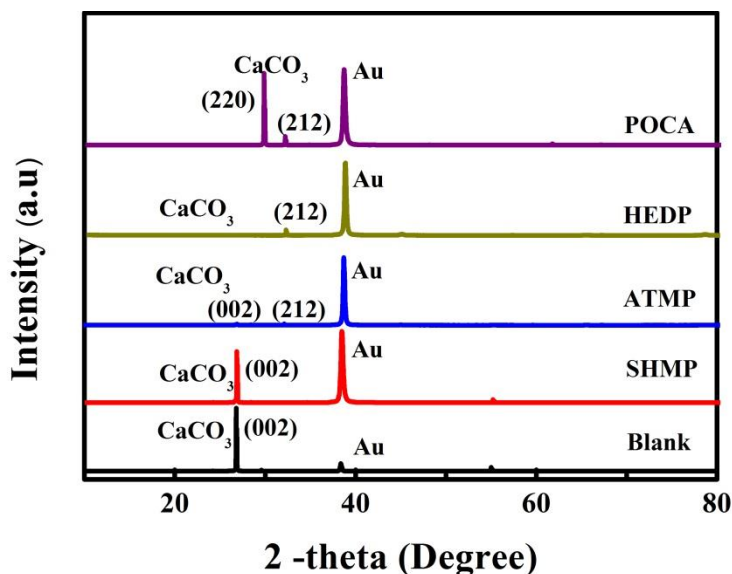


Figure 10. Crystal faces of CaCO_3 obtained from XRD results with and without the presence of a scale inhibitors (10 mg/L): (a) Blank, (b) ATMP, (c) HEDP, (d) POCA, (e) SHMP, scaling temperature (50°C), applied potential ($-1.4\text{ V}_{\text{SCE}}$), scaling time (3600 s).

3.6. Inhibition mechanism

Unlike the classical studies of scale inhibitor in natural scaling processes [18,30], the CaCO_3 crystals obtained in the presence of scale inhibitors using the EQCM system do not show any crystalline phase transformation (i.e., from calcite to vaterite or aragonite), which is revealed by XRD results [calcite-III PDF #17-0763]. This reveals that the scale inhibitors in this study only modify the crystal morphology and particle sizes rather than the CaCO_3 crystalline phase.

For SHMP, the CaCO_3 crystals are similar to those of the blank sample, both in crystal morphology and in particle size. With the inhibition effect of SHMP, there are fewer scale crystals distributing on the gold surface. This means that SHMP only acts as an inhibitor by chelating with Ca^{2+} to form a soluble calcium salt, or by dissolving the active site of a CaCO_3 crystal, which can result in a significant decrease of the surface zeta potential and then inhibit scale formation [29]. Abd-El-Khalek claims that SHMP, at a low concentration of 2 ppm, prevents the total coverage stage of the electrode surface in the scaling process by prolonging the nucleation period [31], which may explain its inhibition mechanism, too. In addition, similar to the blank sample, the scale crystals grow preferentially along the (002) plane laterally, and a regular rhombohedral shape is formed. This reveals that SHMP mainly shows a global inhibition effect for CaCO_3 scale nucleation rather than restraining the growth of crystals or affecting the crystal morphology. As a result, the scale particles formed in the SHMP-containing solution are ‘few in number but large in size’.

In the case of ATMP, the growth of CaCO_3 crystals may be determined by growth competition on different crystal faces. According to the Bravais rule, the growth and morphological changes of crystals, are mainly attributed to the comparative growth rates on every crystal face. In this situation, competition between the (002) and (212) planes and other obscure planes determines the morphology

of the CaCO_3 crystals. The phosphonate molecules of ATMP adsorb preferentially on the kinks or steps of certain crystal faces, thereby modifying the growth rates along certain directions. Thus, the global growth rate decreases abruptly as one face of the CaCO_3 crystal interrupts its growth [28]. With the growths along the (002) and (212) planes being retained, the difference between these two planes finally leads to a column-like shape of the CaCO_3 crystal. This is different from using the bubbling method to measure the inhibition of ATMP in which the CaCO_3 exhibits a fractured lump shape [23].

With the involvement of HEDP, the (212) plane becomes the preferred plane of the CaCO_3 crystals. This means that the growth direction of CaCO_3 crystals is along the direction of the (212) plane. As a result, the shape of the scale tends to be plate-like. Moreover, HEDP inhibits the formation of CaCO_3 not only by chelating with Ca^{2+} and removing the active sites but also by distorting the growth of CaCO_3 crystals both with respect to morphology and particle size. The morphologies of CaCO_3 crystals in the presence of HEDP are also different at different concentrations. For example, in the presence of HEDP (0.7 mg/L) the crystals are composed of a rhombohedral part continued by two symmetrically opposed elongated parts in the EQCM test [28], while it appears as a deformed hexagon (0.5 mg/L), rod-like (1.0 mg/L) and disk-like (1.5 mg/L) in the natural scaling process [30]. It seems that this is an interesting insight into the effect of the inhibitor concentration for investigation in the future.

Regarding the case of POCA, the (220) and (212) planes become the preferential planes of CaCO_3 crystals. There is an enormous ratio of crystallinity between these two planes, indicating the difference of comparative growth rates along these two planes. Hence the obvious growth distinction results in an irregular rhombohedral structure with a void in the CaCO_3 crystal. It was reported that a polymeric phosphate scale inhibitor inhibits the scaling of CaCO_3 mostly by dispersing CaCO_3 scale to prevent its deposition, which explains the inhibition efficiency diversity between the inhibition measurement and kinetic study of POCA. At the free scaling time of 900 s (the end of region 1), the addition of POCA disorganizes the deposition of the CaCO_3 precipitate. In addition, POCA also exhibits an incredible lattice distortion ability. Comparatively, the crystal shape tends to be flower-like in the natural scaling process when these polymer scale inhibitors are used. This is due to the elongation of the agglomerated aragonite structure that forms a prolate sphere morphology [32].

4. CONCLUSIONS

In this paper, EQCM was used to investigate the scaling process in different conditions. SEM and XRD were also used to analyze the scaling mechanism. The study's conclusions are the following:

1. As the temperature rises, the growth rate of scaling rapidly increases, which obeys the Arrhenius equation and has an E_a value of 12.73 kJ/mol. Applied potential also shows a positive correlation with growth rate and the cathode current density, calculated by the electro-deposition equation, is 69.71%.

2. In inhibition measurement, the growth rate or inhibition efficiency reaches a peak value at approximately 10 mg/L for HEDP and SHMP. For ATMP and POCA, the inhibition efficiency

increases with increasing concentration of scale inhibitors. HEDP shows the best inhibition efficiency among the four scale inhibitors at the concentration of 10 mg/L. The order of performance of the four scale inhibitors, ranging from high to low, is HEDP, SHMP, POCA and ATMP. The growth rates of CaCO_3 under the inhibition of POCA, HEDP and ATMP are at almost the same order of magnitude and the inhibition efficiency, ranging from high to low, is POCA, ATMP and HEDP.

3. POCA has a strong effect on the lattice distortion of CaCO_3 crystals but a weak effect on particle size. ATMP and HEDP show significant influences both on crystal morphology and particle size. In contrast, SHMP does not restrain the growth of crystals or affect crystal morphology. The preferred crystal plane of scale without a scale inhibitor is the (002) plane. This plane does not change in the presence of SHMP, while it changes to the (002) and (212) planes for ATMP, the (212) plane for HEDP, and the (220) and (212) planes for POCA.

References

1. G. Gauthier, Y. Chao, O. Horner, O. Alos-Ramos, F. Hui, J. Lédion, H. Perrot, *DES.*, 299 (2012) 89.
2. H. Li, M. K. Hsieh, S. H. Chien, J. D. Monnell, D.A. Dzombak, R.D. Vidic, *Water Res.*, 45 (2011) 748.
3. Q. Yang, *Chem. Eng. Sci.*, 57 (2002) 921.
4. J. MacAdam, S. A. Parsons, *Water Sci. Technol.*, 49 (2004) 153.
5. A. Antony, J. H. Low, S. Gray, A. E. Childress, P. Le-Clech, G. Leslie, *J. Membr. Sci.*, 383 (2011) 1.
6. F. Hui, J. Lédion, *J. Eur. J. Water Qual.*, 33 (2002) 41.
7. C. Gabrielli, M. Keddani, A. Khalil, G. Maurin, H. Perrot, R. Rosset, M. Zidoune, *J. Electrochem. Soc.*, 145 (1998) 2386.
8. J. Lédion, P. Leroy, J.P. Labbe, *Techniques Etences Municip-ales*, 80 (1985) 323.
9. N. Abdel-Aal, K. Satoh, K. Sawada, *Anal. Sci.*, 17 (2001) 825.
10. I. Ben Salah, M. M. Tlili, M. Benamor, *Eur. J. Water Qual.*, 41 (2010) 51.
11. T. A. Hoang, H. M. Ang, A. Rohl, *Powder Technol.*, 179 (2007) 31.
12. C. Gabrielli, G. Maurin, H. Perrot, G. Poindessous, R. Rosset, *J. Electroanal. Chem.*, 538 (2002) 133.
13. O. Devos, C. Gabrielli, B. Tribollet, *J. Cryst. Growth.*, 52 (2006) 285.
14. D. Liu, W. Dong, F. Li, F. Hui, J. Lédion, *J. DES.*, 304 (2012) 1.
15. R. Ketrane, B. Saidani, O. Gil, L. Leleyter, F. Baraud, *DES.* 249 (2009) 1397.
16. C. Gabrielli, M. Keddani, H. Perrot, A. Khalil, R. Rosset, M.Zidoune, *J. Appl. Electrochem.*, 26 (1996) 1125.
17. C.G. Kontoyannis, N.V. Vagenas, *Analyst.*, 125 (2000) 251.
18. Y. M. Al-roomi, K. F. Hussain, M. Al-rifaie, *DES.*, 375 (2015) 138.
19. D. Peronno, H. Cheap-charpentier, O. Horner, *J. Water Process Eng.* 2015, 7, 11.
20. L. M. Feng, *Beijing: Chemical Industry*, (2005) 3.
21. M.M. Tlili, M. Benamor, C. Gabrielli, H. Perrot, B. Tribollet, *J. Electrochem. Soc.*, 150 (2003) 765.
22. C. Deslouis, *J. Appl. Electrochem.*, 27 (1997) 482.
23. Y. Tang, W. Yang, X. Yin, Y. Liu, P. Yin, J. Wang, *DES.*, 228 (2008) 55.
24. A.G. Xyla, J. Mikroyannidis, P.G. Koutsoukos, *J. Colloid Interface Sci.*, 153 (1992) 537.
25. Z. G. Cai, J. Ge, M. Q. Sun, B.L. Pan, T. Mao, Z. Z. Song, *Sci. China B Chem.*, 50 (2007) 114.

26. S. Gopi, V. K. Subramanian, K. Palanisamy, *Mater. Res. Bull.*, 48 (2013) 1906.
27. P. Zhang, G. G. Qian, Z. P. Xu, H. S. Shi, J. Yang, R. L. Frost, *J. Colloid Interface Sci.*, 367 (2012) 264.
28. C. Garcia, G. Courbin, F. Ropital, C. Fiaud, *Electrochim. Acta.*, 46 (2001) 973.
29. J. X. Guo, J. J. Cao, M. Y. Li, H. Y. Xia, F. Lqklelwru, V. Lqklelwru, W. K. H. Rloilhogy, *Pet. Sci.*, 10 (2013) 415.
30. G. C. Zhang, J. J. Ge, M. Q. Sun, B. L. Pan, M. Tao, Z. Z. Song, *Sci. China ser. B*, 50 (2007).1).
31. D. E. Abd-el-khalek, B. A. Abd-el-nabey, *DES*, 311 (2013) 227.
32. H. Ou, L. C. Hsieh, *Powder technol.*, 302 (2016) 160.

© 2017 The Authors. Published by ESG (www.electrochemsci.org). This article is an open access article distributed under the terms and conditions of the Creative Commons Attribution license (<http://creativecommons.org/licenses/by/4.0/>).